Structural and Dynamical Changes of the Bindin B18 Peptide upon Binding to Lipid Membranes. A Solid-State NMR Study†

Patrick Barré,‡,§ Olaf Zschörnig,‡ Klaus Arnold,‡ and Daniel Huster*,§

Institute of Medical Physics and Biophysics, University of Leipzig, and Junior Research Group Solid-State NMR Studies of the Structure of Membrane-Associated Proteins, Biotechnological−Biomedical Center of the University of Leipzig, Liebigstrasse 27, D-04103 Leipzig, Germany

Received February 11, 2003; Revised Manuscript Received May 14, 2003

ABSTRACT: Structural and dynamical features of the B18 peptide from the sea urchin sperm bindin protein were determined in the crystalline state and in zwitterionic lipid bilayers at a peptide:lipid molar ratio of 1:12 using solid-state NMR spectroscopy. The study was focused on three ^{13}C and ^{15}N uniformly labeled leucine residues, which were introduced into three different B18 peptides at positions evenly distributed along the B18 primary structure. Isotropic ^{13}C and ^{15}N chemical shift measurements showed that while B18 possesses a nonhelical and non-sheet-like structure in the crystalline state, the peptide adopts an oligomeric β-sheet structure in the membrane in the presence of Zn^{2+} ions at high peptide:lipid ratio. Torsion angle measurements for the three leucine sites supported these results, with ϕ torsion angles between −80° and −90° in the crystalline state and between −110° and −120° in the membrane-bound form. These ϕ torsion angles determined for membrane-bound B18 are consistent with a parallel β-sheet secondary structure. Analysis of motionally averaged dipolar coupling measurements established an increase of the mobility in the leucine side chains upon binding to the membrane, whereas the backbone mobility remained essentially unchanged, except in the binding site of Zn^{2+} ions. This difference in mobility was related to the H-bond network in the parallel β-sheet structure, which involves the backbone and excludes the side chains of leucine residues. The parallel β-sheet structure of B18 in the membrane in the presence of Zn^{2+} appears to be an active state for the fusion of zwitterionic membranes in the presence of Zn^{2+}. A fluorescence fusion assay indicated that high B18 concentrations are required to induce fusion in these systems. Therefore, it was hypothesized that the oligomeric β-sheet secondary structure revealed in the study represents an active state of the peptide in a membrane environment during fusion.

Membrane fusion events are key processes in cellular life involving for instance endo- or exocytosis, membrane recycling, fertilization, and enveloped virus infection (*1*). Before fusion can occur, close approach and contact between the membranes have to be established. However, a number of repulsive surface forces such as hydration and electrostatic interactions as well as steric barriers act against the close approach of the opposing membranes (*2*). In biological cells, these repulsive surface forces can be overcome by the action of a machinery of fusion proteins (*3*). Thus, close approach between the opposing surfaces is facilitated by protein-induced local dehydration and charge compensation while steric barriers are defeated by local perturbations and destabilizations of the bilayer structure induced by fusion proteins.

Typically, these fusion proteins are large membrane-stemming molecules that contain a relatively short peptide sequence playing the decisive role in the fusion event (*4*). These fusion peptides consist of approximately 20−30 amino acids and have been shown to induce membrane fusion in model systems. A large structural variety has been observed for fusion peptides in model systems with bilayer membranes (*5*−*10*). It turned out that the α-helical conformation appears to be more prevailing than the β-sheet structures (*1*). Investigating the action of fusion peptides on membranes during fusion events, it is interesting to note that the biologically active state appears to be manifested by self-aggregation and oligomerization of the fusogenic peptides (*8*, *11*).

One peptide that has been shown to induce fusion in vesicle systems is the B18[1] from the 25 kDa fertilization protein bindin, which mediates fusion between sperm and

† This work was supported by the Deutsche Forschungsgemeinschaft (Ar-195/8-1). The junior research group is funded by the Saxon State Ministry of Higher Education, Research, and Culture.

* Corresponding author. Tel:+49 (0) 341-97-15706. Fax: +49 (0) 341-97-15709. E-mail: husd@medizin.uni-leipzig.de.

‡ Institute of Medical Physics and Biophysics, University of Leipzig.

§ Biotechnological−Biomedical Center of the University of Leipzig.

[1] Abbreviations: B18, 18 amino acid peptide from the bindin protein (residues 103−120) with an amino acid sequence of LGLLL RHLRH HSNLL ANI; CD, circular dichroism; CP, cross-polarization; DIP-SHIFT, dipolar coupling and chemical shift correlation; FSLG, frequency-switched Lee−Goldburg; HNCH, $^{1}H-^{15}N-^{13}C-^{1}H$ correlation experiment for ϕ torsion angle determination; HSQC, heteronuclear single-quantum coherence; LUV, large unilamellar vesicles; MAS, magic angle spinning; MLV, multilamellar vesicles; NBD-PE, *N*-(7-nitro-2,1,3-benzoxadiazol-4-yl)phosphatidylethanolamine; POPC, 1-palmitoyl-2-oleoyl-*sn*-glycero-3-phosphocholine; POPC-d_{31}, 1-palmitoyl-d_{31}-2-oleoyl-*sn*-glycero-3-phosphocholine; REDOR, rotational echo double resonance; Rh-PE, *N*-(lissamine Rhodamine B sulfonyl)phosphatidylethanolamine; RMSD, root-mean-square deviation; TFE, trifluoroethanol; TPPM, two pulse phase modulation; FTIR, Fourier transform infrared; FRET, fluorescence resonance energy transfer.

10.1021/bi034239e CCC: $25.00
Published on Web 06/17/2003

egg cells. Bindin is located in the membranes of sperm cells of sea urchin (*12*, *13*). The role of bindin in the fusion event of egg and sperm cell has been determined in model experiments probing fusion of lipid vesicle systems (*14*−*17*). The central part of the protein consists of a highly conserved hydrophobic region of about 70−80 residues. Within that region, an 18 amino acid peptide (residues 103−120), which is fully conserved in all sea urchin species, appears to represent the minimum sequence capable of inducing membrane fusion (*18*). This peptide, called B18, shows an affinity for lipid membranes, is capable of aggregating and fusing lipid bilayers, and binds Zn^{2+} by a His-rich central motif in the B18 sequence (*18*). The presence of Zn^{2+} ions strongly enhances the fusion activity of the peptide for zwitterionic membranes while little effect is observed in the absence of Zn^{2+} (Zschörnig et al., in preparation).

In aqueous solution, B18 is largely unstructured as indicated by circular dichroism (CD) experiments (*18*). Upon Zn^{2+} binding, B18 appears to undergo a structural change from unstructured to α-helical as observed by CD. The peptide structure has been further characterized in a solution NMR study revealing that B18 assumes a kinked α-helical structure in TFE solution or when bound to DPC or SDS micelles, but the B18 peptide remains unstructured in aqueous solution (*19*). In the presence of Zn^{2+}, the kinked helix becomes amphipathic, suggesting that the peptide might favorably penetrate into a lipid bilayer.

Further structural characterization of the peptide has been carried out in a Fourier transform infrared (FTIR) spectroscopy approach (*20*). Using the attenuated total reflection FTIR technique, the effect of Zn^{2+} on the secondary structure of B18 and its interaction with lipid bilayer membranes could be investigated. In good agreement with the CD results, the peptide was found to have a largely random structure in the absence of Zn^{2+} but becomes α-helical when Zn^{2+} is added. When added to POPC membranes, the measurements revealed an α-helical structure of B18 at a molar ratio of 1:50. On the other hand, the FTIR spectra of B18 at a much higher molar ratio of 1:5 with POPC showed the characteristic features of a *β*-sheet conformation (*20*). This is in agreement with freeze−fracture electron microscopy data indicating that the peptide shows a preference for *β*-sheet structures at higher concentrations (molar ratios of peptide to lipid of 1:10) (*21*).

In this study, the structure and dynamics of B18 have been investigated by solid-state NMR in both the presence and absence of phospholipid membranes. The advantage of solid-state NMR is that intact lipid bilayers with the peptide incorporated can be investigated, which are more biologically relevant than detergent micelles. The tradeoff is the spectral resolution that suffers from broad signals due to anisotropic chemical shifts and dipolar couplings. However, by application of magic angle spinning (MAS) and high-power decoupling, sufficiently well-resolved ^{13}C NMR spectra are obtained (*22*). Despite these technical difficulties, significant advances have been achieved in the last years to investigate the structure and dynamics of membrane-associated peptides and proteins (*23*−*27*). In particular, specific isotopic labeling schemes allow determination of quantitative structural constraints such as distances or torsion angles as well as dynamical parameters of membrane-associated peptides and proteins with great precision.

So far, only a few solid-state NMR studies of membrane-bound fusion peptides have been carried out (*6*, *28*). In this work, we performed solid-state NMR measurements to investigate the structure and dynamics of membrane-bound B18 under conditions relevant for membrane fusion, i.e., in the presence of Zn^{2+} ions. Three different peptides were synthesized, each bearing a fully $^{13}C/^{15}N$-labeled Leu residue in the structure. Thus, site-specific structural information is obtained to better understand the biological action of the peptide when interacting with the lipid membrane.

EXPERIMENTAL PROCEDURES

Materials. The lipids 1-palmitoyl-2-oleoyl-*sn*-glycero-3-phosphocholine (POPC), 1-palmitoyl-d_{31}-2-oleoyl-*sn*-glycero-3-phosphocholine (POPC-d_{31}), *N*-(7-nitro-2,1,3-benzoxadiazol-4-yl)phosphatidylethanolamine (NBD-PE), and *N*-(lissamine Rhodamine B sulfonyl)phosphatidylethanolamine (Rh-PE) were purchased from Avanti Polar Lipids, Inc. (Alabaster, AL) and used without further purification. Fmoc-[U-^{13}C,^{15}N]Leu was purchased from Cambridge Isotopes, Inc. (Andover, MA). The B18 peptide with the amino acid sequence LGLLL RHLRH HSNLL ANI was synthesized at the Medical Faculty (Charité) of Humboldt University Berlin by the standard Fmoc peptide synthesis protocol. Each peptide, named hereafter B18 L-*n* with $n = 4$, 8, or 15, contained one uniformly ^{13}C- and ^{15}N-labeled leucine that was inserted at the *n*th position of the peptide sequence.

Sample Preparation. For solution NMR measurements, 1 mg of B18 was dissolved in 1 mL of aqueous buffer (10 mM NaCl, 10 mM Hepes, pH 7.4) prepared from a 90/10 (v/v) H_2O/D_2O mixture. For the crystalline samples, approximately 30 mg of peptide powder was filled into a 4 mm MAS rotor with Teflon insert.

For the membrane-bound samples liposomes were prepared by vortexing the aliquots of POPC in buffer (10 mM HEPES, 10 mM NaCl, pH 7.4) at a concentration of about 50 mg/mL. The suspension was submitted to 10 freeze−thaw cycles for equilibration. Large unilamellar vesicles (LUV) were prepared by extrusion across a polycarbonate Unipore membrane (100 nm pore size; Millipore Corp., Bedford, MA) using a Lipex extruder (Biomembranes, Vancouver, British Columbia, Canada) (*29*). The lipid concentration after extrusion was measured by phosphorus determination (*30*). The B18 peptide, dissolved in buffer, was added to the suspension to reach the desired peptide to lipid molar ratio. Subsequently, zinc ions were added at a 5 mM concentration, and the mixture was lyophilized. After lyophilization, the sample was rehydrated to a water content of 30 wt % and equilibrated by freeze−thaw cycles, stirring, and gentle centrifugation. The sample was finally transferred into a 4 mm MAS rotor with Teflon inserts (50 *μ*L volume) for NMR measurements.

Solution NMR Spectroscopy. Solution NMR experiments were performed on a DRX600 spectrometer (Bruker Biospin, Rheinstetten, Germany), operating at a resonance frequency of 600.13 MHz for ^1H and 150.91 MHz for ^{13}C. Sensitivity-enhanced gradient heteronuclear single-quantum coherence (HSQC) spectra (*31*) were acquired, using 90° pulse lengths of 8.2 and 14.5 *μ*s for ^1H and ^{13}C, respectively.

Static Solid-State NMR Experiments. ^2H NMR spectra were acquired on a Bruker DMX300 spectrometer, operating

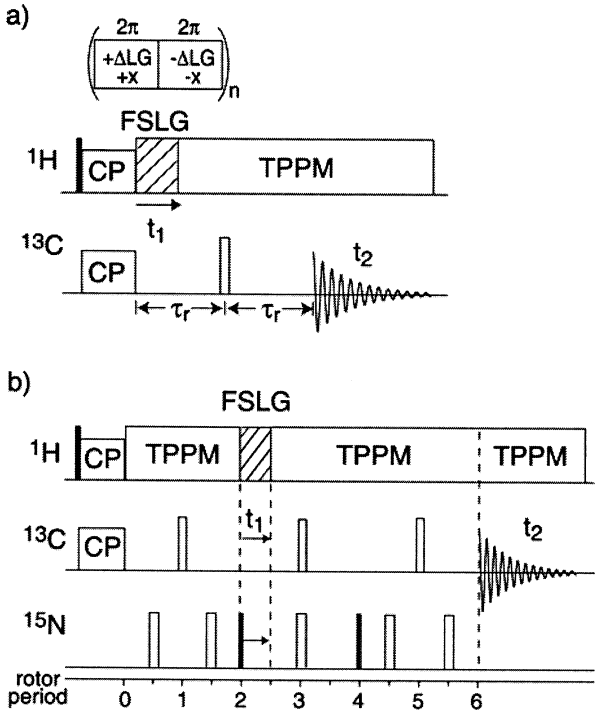

FIGURE 1: Pulse sequences of the constant time DIPSHIFT (a) and the HNCH experiment (b) applied to investigate molecular order parameters and local secondary structure of peptides. Filled and open rectangles represent $\pi/2$ and π pulses, respectively. Key: CP, cross-polarization; TPPM, two pulse phase modulation decoupling; FSLG, frequency-switched Lee−Goldburg decoupling; τ_r, length of a rotor period.

at a resonance frequency of 46.06 MHz. A high-power probe with a 5 mm solenoid coil was used. Spectra were acquired using a phase-cycled quadrupolar echo pulse sequence (*32*) with two 4.8 μs 90° pulses, a 100 μs delay between pulses, and a relaxation delay of 0.5 s. The carrier frequency was placed at the center of the spectrum.

Data analysis was carried out as described in ref *33*. The treatment involved the dePaking of the real part of the spectra using the algorithm of McCabe and Wassall (*34*) to determine the order parameter of each individual methylene group in the lipid chain.

MAS NMR Experiments. All solid-state MAS NMR experiments were carried out on a Bruker AVANCE 750 spectrometer at a resonance frequency of 749.98 MHz for ^{1}H, 188.62 MHz for ^{13}C, and 76.01 MHz for ^{15}N. A triple-resonance MAS probe was used for torsion angle measurements, whereas dipolar coupling measurements were carried out using a double-resonance MAS probe, both equipped with a 4 mm spinning module.

CP MAS spectra were acquired using a ^{1}H 90° excitation pulse of 4−4.5 μs length and a cross-polarization (CP) contact time of 700 μs for ^{13}C and 2 ms for ^{15}N. The ^{1}H radio-frequency field strength for heteronuclear two pulse phase modulation (TPPM) decoupling (*35*) was between 55 and 65 kHz.

The strength of the ^{15}N−^{1}H and the ^{13}C−^{1}H dipolar couplings was measured using the constant time dipolar and chemical shift (DIPSHIFT) pulse sequence (*36*−*38*) (Figure 1a). The strengths of these coupling values are crucial input parameters for the simulations necessary for the determination of the torsion angle ϕ (see below). They also provide information about the dynamics of the peptide under study. For the DIPSHIFT experiment, ^{1}H−^{1}H homonuclear decoupling was achieved with the frequency-switched Lee−Goldburg (FSLG) sequence (*39*). The 360° ^{1}H pulses had a duration of 15−18 μs, with an effective decoupling field strength of 70−80 kHz. The MAS frequencies were 7000 Hz for ^{13}C and 5000 Hz for ^{15}N DIPSHIFT experiments. Since the dipolar-induced signal decay is periodic with the rotor period, it was only necessary to acquire the signal over one rotor period in the indirect dimension. Therefore, DIPSHIFT spectra were only Fourier transformed in the direct dimension, and the dipolar dephased signal was extracted for each resolved peak. The one-rotor-period time domain data were fitted to yield the coupling strength of interest.

The torsion angle ϕ was determined using the HNCH pulse sequence (*38*) (Figure 1b). After a first REDOR period, during which the dipolar coupling between ^{13}C and ^{15}N is reintroduced under MAS conditions, heteronuclear multiquantum coherences of the C_xN_y type are created. These coherences are allowed to evolve simultaneously under the influence of the ^{1}H−^{13}Cα and the ^{1}H−^{15}N dipolar coupling tensors during t_1. This dephasing of the MAS signal during one rotor period depends on the respective orientation of the tensors that are aligned along the Cα−H and N−H bonds. Thus, the evolution is related to the projection angle between the Cα−H and N−H bonds, ϕ_H, which provides the ϕ torsion angle since $\phi_H = \phi - 60°$ for L-amino acids. This results in the encoding of the coherences with torsion angle information. These coherences are converted to ^{13}C observable magnetization using an additional REDOR sequence and detected during t_2.

The ^{13}C and ^{15}N 180° pulse lengths were 12 and 13 μs, respectively. All other parameters were akin to the CP and the DIPSHIFT experiments. The samples were spun at a $\omega_r/2\pi = 4000$ Hz rate. The number of scans was between 2K and 5K for the crystalline and between 4K and 10K for the membrane-bound samples. Again, due to the periodicity of the signal, acquisition only lasted one rotor period in the indirect dimension. A dephasing curve was obtained after Fourier transform in the direct dimension only. These data were fitted to yield the torsion angle.

Simulations. The time evolution under the C−H (or N−H) dipolar couplings in 2D DIPSHIFT experiments was simulated for one rotor period using Mathcad (Mathsoft, Inc., Cambridge, MA). Simulations were performed for varying dipolar coupling strengths. Powder averaging was performed in 2° and 3° increments for the β and γ Euler angles, respectively. Other input parameters included the number of t_1 increments, the dwell time, and the spinning rate.

The time evolution under the influence of the Cα−H and N−H dipolar coupling tensors in torsion angle measurements was simulated with a Fortran program described in ref *38*. Input parameters were the spinning rate, the number of time domain points, and the $\delta_{C\alpha-H}$ and δ_{N-H} coupling constants, measured in the DIPSHIFT experiments. Powder averaging was performed in 3° increments for all three Euler angles.

For all experiments, the simulated curves were multiplied with an exponential decay to account for T_2 relaxation effects during the time evolution. The best agreement between simulation and experiment was determined by the smallest RMSD values.

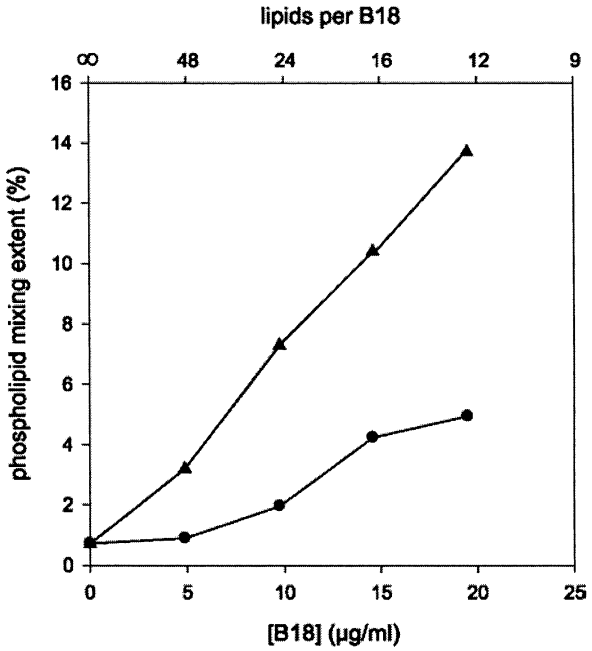

FIGURE 2: Phospholipid mixing extents in LUV according to the NBD-Rh FRET experiment as a function of the B18 concentration. Fluorescence experiments were carried out at Zn^{2+} concentrations of 50 μM (▲) and 5 μM (●) at a temperature of 30 °C. Buffer concentration: 100 mM NaCl and 10 mM Hepes, pH 7.4.

Phospholipid Mixing Experiments. For the investigation of fusogenic activity of B18, POPC LUV were prepared containing 1 mol % of NBD-PE and Rh-PE, respectively. The mixing of phospholipids as a result of fusion was followed by the fluorescence resonance energy transfer (FRET) method, using NBD-PE as donor and Rh-PE as acceptor (*40*, *41*). The fluorescence measurements were carried out using an excitation wavelength of 465 nm; fluorescence emission was recorded from 500 to 620 nm. The fluorescence intensities reached equilibrium after about 1 min. The extent of phospholipid mixing *M* was calculated from the intensity of NBD-PE at 525 nm and Rh-PE at 578 nm according to

$$M = \frac{I_{525}}{I_{578}} - \frac{I^0_{525}}{I^0_{578}} \quad (1)$$

where *I* is the fluorescence intensity in the presence and I^0 that in the absence of B18. The experiments were carried out at 30 °C. The 100% value of PL mixing was obtained by solubilization of the vesicles in 0.2% (v/v) Triton X-100.

RESULTS

B18-Induced Fusion of POPC Vesicles. The purpose of this study was to investigate structural and dynamical aspects of B18 interaction with zwitterionic membranes in the presence of Zn^{2+} using solid-state NMR methods. To find out the critical B18 concentration for fusogenic activity, the fusion activity of B18 for POPC membranes in the presence of Zn^{2+} was investigated by a fluorescence assay using FRET. Figure 2 shows the phospholipid mixing extent of the NBD-Rh mixing assay for the B18/POPC/Zn^{2+} system in a concentration regime marking the onset of phospholipid intermixing. For both Zn^{2+} concentrations, an increase of the phospholipid mixing extent as a result of vesicle fusion is observed. As indicated from the measurements, it is to be expected that the fusion extent increases for higher B18 concentration; however, here, we were only interested in finding the critical B18 concentration to induce vesicle fusion. For instance, if we define a phospholipid mixing extent of 10% as a threshold value for fusion activity, a B18 concentration of approximately 15 μg/mL is required at 50 μM Zn^{2+}. This also appears to be the threshold concentration for the onset of POPC fusion at low Zn^{2+} concentration. This translates into 16 POPC molecules per B18 and even fewer lipids per B18 if one only considers the outer membrane leaflet. Therefore, a rather high B18:phospholipid ratio is required to induce appreciable amounts of fusion in zwitterionic POPC membranes.

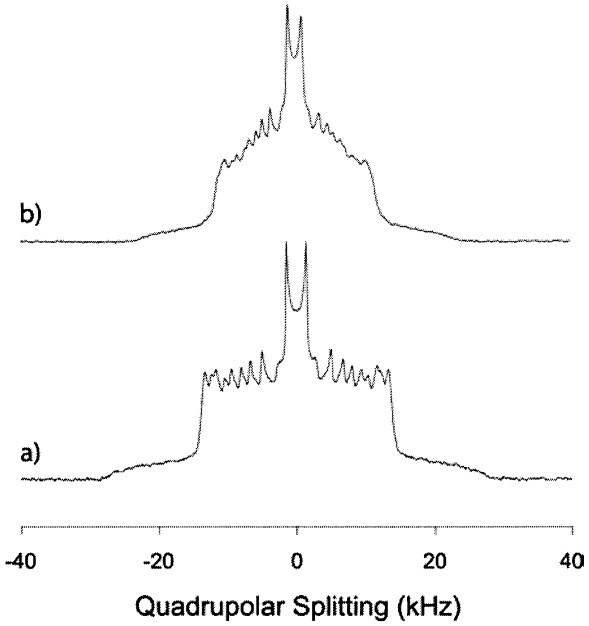

FIGURE 3: 46.1 MHz ^{2}H NMR spectra of POPC-d_{31} in the absence (a) and presence (b) of B18 at a temperature of 25 °C and a lipid to peptide molar ratio of 12:1. Measurements were performed in 30 wt % aqueous buffer (10 mM NaCl, 5 mM $ZnCl_2$, 10 mM Hepes, pH 7.4).

Therefore, we constructed the system for B18 structural and dynamical studies at a relatively high B18:POPC mixing ratio of 1:12. A Zn^{2+} concentration of 5 mM was used, translating into 1.5 Zn^{2+} ions per B18 molecule.

^{2}H NMR Spectra and Chain Order Parameters. Static solid-state ^{2}H NMR spectra of pure POPC membranes (a) and POPC membranes with associated B18 (b) both in the presence of 5 mM Zn^{2+} are shown in Figure 3. Eight well-resolved quadrupolar splittings were observed. The effect of B18 binding is unmistakable in the drastic reduction of all quadrupolar splittings that is observed in Figure 2b. Addition of 5 mM Zn^{2+} alone has only a negligible influence on the ^{2}H NMR spectra of POPC (not shown).

To further illustrate the drastic influence of B18 binding on lipid chain order, the ^{2}H NMR spectra of Figure 3 were converted into individual chain order parameters for each deuteron along the chain by the dePaking method. This procedure yields order parameter profiles shown in Figure 4. The reduction in POPC chain order due to B18 binding is experienced for all molecular segments of the POPC chains. Thus, the average order parameter decreased from 0.172 in

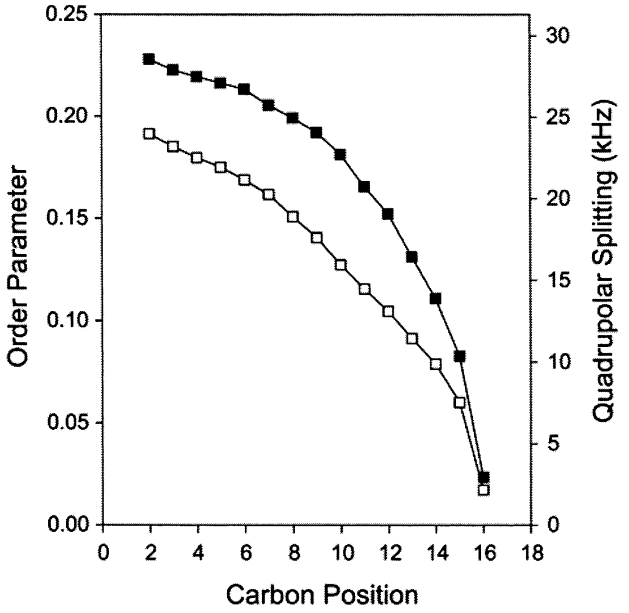

FIGURE 4: ^{2}H NMR order parameter profile of the *sn*-1 chain of POPC-d_{31} membranes in the absence (■) and presence (□) of the B18 peptide at 25 °C. The experimental conditions were as in Figure 3.

pure POPC membranes to 0.132 in the B18-associated POPC MLVs. This loss of order leads to a decrease of the molecular packing density and an increase in the area per POPC molecules in the membrane, which can be quantified according to ref *42*. From the changes in lipid chain order, an increase of area per molecule of 4.3 Å^2 was calculated.

^{13}C NMR Isotropic Chemical Shifts. ^{13}C CP MAS and ^{13}C HSQC NMR spectra of crystalline B18 L-8, B18 L-8 bound to POPC membranes in the presence of 5 mM Zn^{2+}, and B18 L-8 in aqueous buffer are shown in Figure 5. The peaks marked with a B or L were assigned to buffer signals in HSQC spectra (c) and to lipid signals in MAS spectra (b), respectively. The typical line width for the ^{13}C/^{15}N-labeled Leu in B18 in the CPMAS spectra is about 1.3 ppm for the Cα signal in the absence and about 1.8 ppm in the presence of POPC membranes. For the CO line, the width is between 2.1 and 3.5 ppm in the absence and between 1.3 and 2.1 ppm in the presence of POPC. For comparison, the relatively mobile lipid molecules exhibit signals with a width of less than 0.5 ppm. The ^{13}C chemical shifts of the B18 peptides were calibrated with respect to the ^{13}CO signal of an external ^{13}C-labeled glycine standard in all three spectra. Amidic ^{15}N chemical shifts of labeled leucines in B18 were also determined in the crystalline and the membrane-bound states (spectra not shown) and referenced with respect to the ^{15}N *N-t*-Boc-Gly signal.

Isotropic chemical shifts are sensitive markers for secondary structure (*43*, *44*). For instance, compared to the random coil chemical shift, a downfield shift of the ^{13}C Cα signal with a simultaneous upfield shift of the Cβ signal is indicative of an α-helix formation while the opposite chemical shift changes are signatures of β-sheet structures (*44*). For the ^{15}N amide signal of a protein, β-sheet structures are found at low field while α-helix signals are detected at higher field (*45*).

The isotropic chemical shifts for the Leu in three positions of B18 are shown in Table 1. Several trends for secondary

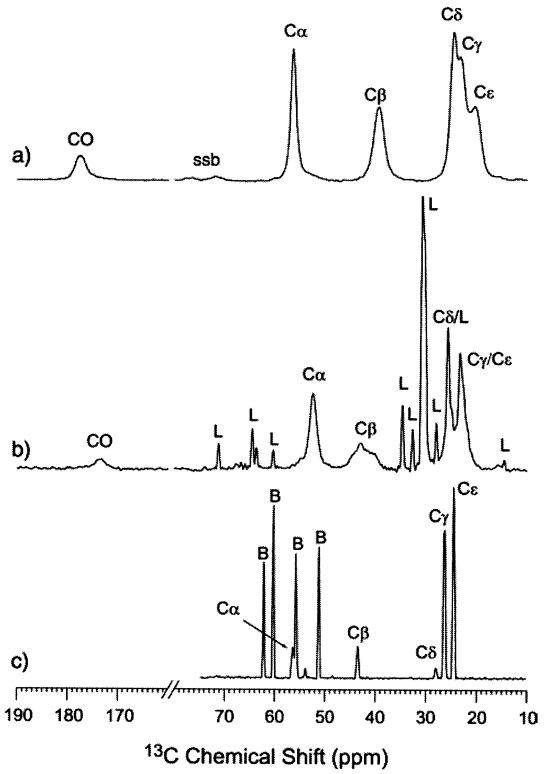

FIGURE 5: 188.6 MHz ^{13}C CP MAS spectra of (a) crystalline B18 L-8 in the absence of water and (b) B18 L-8/POPC membranes (molar ratio of 1:12) at a buffer content of 30 wt % (10 mM NaCl, 5 mM $ZnCl_2$, 10 mM Hepes, pH 7.4). The MAS spinning frequency was 7 kHz for both spectra. (c) ^{13}C dimension of a 150.9 MHz HSQC spectrum of 1 mg/mL B18 L-8 in H_2O/D_2O (90/10 v/v) buffer (10 mM NaCl, 10 mM Hepes, pH 7.4). Spectra were referenced with respect to the CO signal of Gly (176.4 ppm) as an external standard. Lipid and buffer signals are marked with L or B, respectively. ssb = spinning sidebands. All spectra were acquired at a temperature of 25 °C.

Table 1: Isotropic Chemical Shift Values (in ppm) for ^{13}C/^{15}N-Labeled Leu in the Three B18 Peptides in Solution and in the Crystalline and Membrane-Bound States

		Cα[a]	Cβ[b]	Cγ	Cδ	Cϵ	CO[c]	^{15}N[d]
B18 L-4	solution	56.3	43.5	28.5	25.9	25.0		
	crystalline	56.3	39.0	25.0	23.0	20.8	176.8	118.5
	POPC/Zn^{2+}, 5 mM	52.2	43.8	25.6	23.2	22.6	172.7	125.7
B18 L-8	solution	56.3	43.7	28.3	26.2	24.7		
	crystalline	56.3	39.4	24.6	23.3	20.4	177.6	120.0
	POPC/Zn^{2+}, 5 mM	52.4	43.2	25.6	23.3	22.7	175.3	129.7
B18 L-15	solution	56.2	43.4	28.3	26.2	24.6		
	crystalline	55.4	39.7	24.6	23.1	20.7	176.4	117.4
	POPC/Zn^{2+}, 5 mM	51.9	43.9	25.6	23.3	21.6	173.0	126.8

[a] Average Leu ^{13}Cα random coil and β-sheet values are 55.7 and 53.9 ppm, respectively (*43*). [b] Average Leu ^{13}Cβ random coil values are 41.9 ppm (*65*). [c] Average Leu ^{13}CO random coil and β-sheet values are 176.9 and 175.5 ppm, respectively (*43*). [d] Average Leu ^{15}N random coil and β-sheet values are 122.2 and 123.1 ppm, respectively (*45*).

shift changes upon membrane binding are evident for all peptides through a comparison of the data of the crystalline or the aqueous samples with the membrane-bound samples.

First, the backbone carbon atoms, i.e., carbonyl groups and Cα, always shifted to lower chemical shift values in the membrane-bound samples. These changes between 2.3 and 4.3 ppm are significant. Simultaneously, the Cβ side-chain

signals shifted to higher chemical shifts by values between 3.8 and 4.8 ppm. Second, a shift to higher frequencies was observed for the ^{15}N amidic nuclei in all three samples upon binding to the membranes. This shift is very substantial as it is comprised between 7.2 ppm for B18 L-4 and 9.7 ppm for B18 L-15. All of these characteristic chemical shift changes clearly are indicative of a structural change from a coil structure in the crystalline toward a β-sheet-like extended structure in the membrane-bound sample. Our absolute ^{13}C chemical shifts agree well with values from empirical databases (*43*) while the absolute values for the measured ^{15}N shifts are systematically bigger (Table 1), which might be related to hydrogen bonding in *N*-*t*-Boc-Gly. Further, recent quantum chemical calculations indicate that ^{15}N chemical shifts are most sensitive to hydrogen bonding (*46*). Therefore, the large downfield shift might be mostly related to hydrogen bonding in the oligomeric β-sheets. Therefore, we can conclude that the two effects (H-bonding plus change to a β-sheet structure) may add and result in large deshielding of the ^{15}N nuclei.

The ^{13}C HSQC spectra of the water-soluble samples gave somewhat different chemical shift values for the side-chain signals while the position of the Cα resonances agrees well with the crystalline sample. Since the Cα chemical shifts are the most sensitive indicators for secondary structure, it can be concluded that the peptide has a coil structure both in the crystalline and in the soluble state, confirming previous studies (*18*, *19*). However, these structures are very likely not the same. In solution, the peptide has a poorly defined structure, while in the crystalline state the structure is well defined (see below). This is for instance indicated by different side-chain shifts. Differences between side-chain chemical shifts in solution and solid state on the order of up to 5.4 ppm (2.4 ppm for Leu) have been observed before for almost all amino acids, while the Cα values typically show a better agreement between solution and solid state (*47*).

Next, the question arises whether the chemical shift values, i.e., the peptide's secondary structure, are dependent on the B18 concentration. Therefore, we carried out isotropic chemical shift measurements as a function of B18 concentration for B18 L-8 in POPC membranes (Figure 6). It is clearly seen that a structural change occurs at higher B18 concentrations, indicated by significant changes in the isotropic chemical shift values toward the β-sheet structure at high peptide to lipid ratio.

ϕ Torsion Angle Measurements. To corroborate the results from the isotropic chemical shift analysis, the ϕ torsion angle was measured for the labeled leucine residue in all three B18 samples, both in the crystalline and in the membrane-bound states, by correlating the ^{15}NH and ^{13}CH dipolar tensors in a HNCH experiment (*38*). Since the mutual orientation between the two dipolar tensors leads to very different characteristic dephasing of the MAS signal, the torsion angle ϕ can be quantitatively determined from the experiment. Due to sensitivity issues, the torsion angle measurement can only be conducted at high peptide concentration.

Figure 7 represents the dephasing curves of B18 L-8 in the crystalline state (filled squares) and in the membrane-bound state (open squares) recorded over one rotor period. Notice that the number of data points for the membrane-bound samples was only half of that for the crystalline sample. This was to avoid prohibitive experimental time due to high signal averaging, which was necessary for the limited amount of labeled residue in the bound state. For the membrane-bound sample, 10 mg of peptide was used, translating into only ~500 μg of ^{13}C/^{15}N-labeled Leu in each sample.

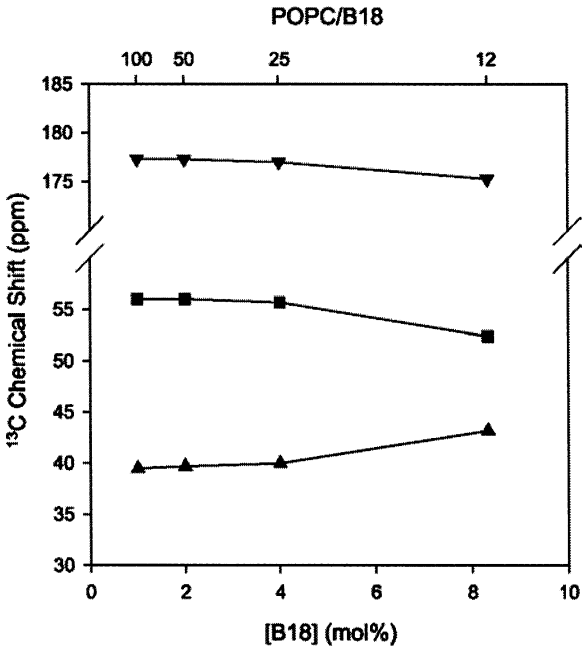

FIGURE 6: ^{13}C isotropic chemical shift values for Cα (■), Cβ (▲), and CO (▼) signals of B18 L-8 in POPC MLV at varying B18 concentration in the presence of 5 mM Zn^{2+} measured from ^{13}C CP MAS spectra at a MAS spinning frequency of 7 kHz at a temperature of 25 °C. Samples were prepared at a buffer content of 30 wt % (10 mM NaCl, 10 mM Hepes, pH 7.4).

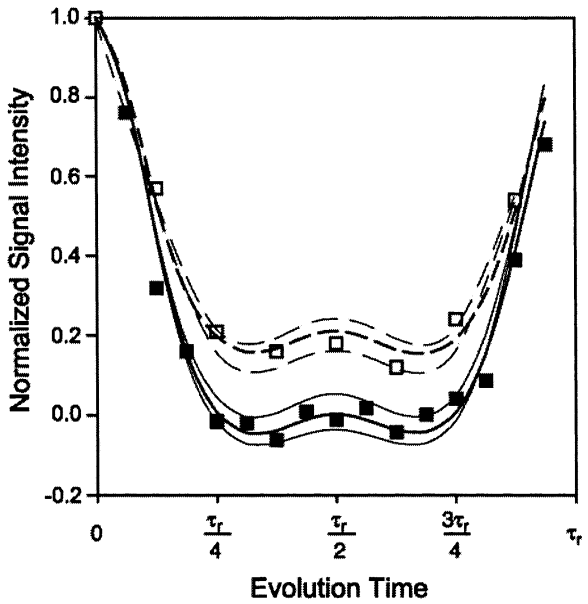

FIGURE 7: Dipolar dephasing curves of HNCH spectra for crystalline B18 L-8 (■) and B18 L-8 bound to POPC membranes in the presence of 5 mM Zn^{2+} at a molar ratio of 1:12 (peptide:lipid) in aqueous buffer (10 mM NaCl, 10 mM Hepes, pH 7.4) (□). Lines represent best fit numerical simulations with ϕ torsion angles of −80° (solid line) in the crystalline and −110° (dashed line) in the membrane-bound state in the presence of 5 mM Zn^{2+}. Somewhat thinner lines that envelop the data points represent simulations with torsion angles ϕ ±10° to indicate the experimental error.

For all three peptides, the dephasing of the MAS signals under the influence of the ^{1}H−^{15}N and ^{1}H−^{13}C dipolar

Table 2: ϕ Torsion Angles (deg) of the B18 Peptides in the Crystalline State and Bound to POPC Membranes in the Presence of 5 mM Zn^{2+} Determined in the HNCH Experiment

	crystalline	POPC/Zn^{2+}, 5 mM
B18 L-4	-80 ± 5	-120 ± 15
B18 L-8	-80 ± 10	-110 ± 10
B18 L-15	-90 ± 5	-120 ± 15

tensors was always less pronounced in the membrane-bound state. To obtain quantitative data for the torsion angle, numerical simulations have been carried out as a function of torsion angle and compared with the experimental data. The best fit (solid line, crystalline B18 L-8; dotted line, membrane-bound B18 L-8) provided the torsion angles reported in Table 2. The torsion angle ϕ was between $-80°$ and $-90°$ in the crystalline state, which agrees with a coil secondary structure. In the membrane-bound state, ϕ torsion angles of $-110°$ and $-120°$ were measured, which represents the torsion angle for parallel β-sheet in the Ramachandran diagram (*48*). The change upon binding with POPC LUV was between 30° and 40° for all Leu residues investigated. This seems to be an indication for a uniform structure of the B18 polypeptide chain, rather than a heterogeneous structure presenting a kink or a loop.

It should be noted that, in the HNCH NMR experiment, the torsion angle $\phi_H = H^N-N-C\alpha-H\alpha$ is measured, which is related to the true backbone torsion angle $\phi = CO-N-C\alpha-CO$ by $\phi_H = \phi - 60°$ for L-amino acids. Each simulation corresponds to two ϕ angles since the NMR experiment determines $\pm\phi_H$. Only the structurally relevant negative ϕ angle has been reported here.

$^1H-^{13}C$ Dipolar Couplings and Order Parameters. To obtain dynamics information for the crystalline and membrane-bound B18 peptides, 2D DIPSHIFT experiments were carried out to measure C−H dipolar couplings of the labeled leucine residues in all three peptides. Since molecular motions partially average dipolar coupling values, these parameters provide order parameters of the amplitude of the motions of the CH bond vectors; the smaller the dipolar coupling, the larger the motional amplitude. Further, the true magnitude of the scaled dipolar CH and NH couplings was used for precise simulations to calculate the ϕ torsion angles from HNCH experiments as described above.

Figure 8 represents typical $^1H-^{13}C$ and $^1H-^{15}N$ dipolar evolution curves for the crystalline (filled squares) and the membrane-bound samples (open squares). The magnitude of the dephasing corresponds to the strength of the dipolar coupling; the more dephasing, the higher the coupling value. The dephasing due to the dipolar interaction is less pronounced for the side-chain signals of membrane-bound samples. Quantitative values for the dipolar coupling strength, obtained from numerical simulations, are listed in Table 3. The measured coupling values are scaled by the scaling factor for the FSLG sequence, which has a theoretical value of 0.577 (*39*). Since this scaling factor varies upon the experimental conditions (*49*), we obtained rigid limit values from measurements of crystalline amino acids as reference values for the full dipolar coupling: CH (Ala, 13.7 kHz), CH_2 (Gly, 16.3 kHz), and CH_3 (Ala, 7.6 kHz) groups. The latter already includes the scaling of the methyl group due to rotation about the C−C bond.

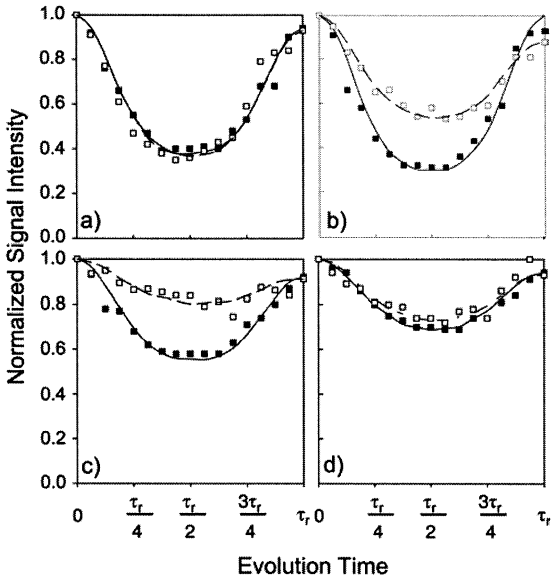

FIGURE 8: Typical $^1H-^{13}C$ and $^1H-^{15}N$ dipolar dephasing curves over one full rotor period of DIPSHIFT spectra of crystalline (■) and membrane-bound B18 L-*n* (□). The four panels show the Cα signal of B18 L-4 (a), the Cβ signals of B18 L-8 (b), the Cγ signals of B18 L-15 (c), and the ^{15}N signal of B18 L-4 (d). Lines represent best fit simulations for the crystalline (solid lines) and the membrane-bound sample (dashed lines). Dipolar coupling values are listed in Table 3.

Table 3: $^1H-^{13}C$ and $^1H-^{15}N$ Dipolar Couplings and CH Order Parameters for Crystalline B18 and B18 Bound to POPC Membranes in the Presence of 5 mM Zn^{2+}

		crystalline		POPC/Zn^{2+}, 5 mM	
		$\Delta\nu_D$	S_{CH}[a]	$\Delta\nu_D$	S_{CH}
B18 L-4	Cα	12.5	0.91	12.6	0.92
	Cβ	14.7	0.90	12.5	0.77
	Cγ	9.4	0.69	9.4	0.67
	Cδ	6.3	0.28	5.1	0.22
	^{15}N	5.5	NA	5.0	NA
B18 L-8	Cα	13.1	0.96	12.1	0.88
	Cβ	13.9	0.85	9.9	0.61
	Cγ	10.5	0.77	5.7	0.42
	Cδ	8.5	0.37	6.2	0.27
	^{15}N	5.7	NA	5.7	NA
B18 L-15	Cα	13.2	0.96	13.0	0.95
	Cβ	13.6	0.83	13.3	0.82
	Cγ	9.8	0.72	5.5	0.40
	Cδ	7.7	0.33	4.3	0.19
	^{15}N	5.2	NA	4.6	NA

[a] The full dipolar coupling values including the FSLG scaling factor were measured from rigid crystalline amino acids: CH, 13.7 kHz; CH_2, 16.3 kHz; and CH_3, 22.8 kHz.

From the motionally averaged dipolar coupling values, the molecular order parameters of the CH bonds (S_{CH}) can be calculated according to

$$S_{CH} = \frac{\bar{\delta}_{CH}}{\delta_{CH}} \qquad (2)$$

where $\bar{\delta}_{CH}$ is the magnitude of the motionally averaged and δ_{CH} the full dipolar coupling.

The general trend for the B18 order parameters indicates that the membrane-associated peptides have higher mobility; i.e., they undergo larger amplitude motions, compared to the crystalline state. This is particularly true for the side chains,

where significantly reduced order is obtained for most signals. It appears that the backbone Cα order parameter remained essentially unchanged, with the notable exception of B18 L-8, for which it decreased from 0.96 in the crystalline state to 0.88 in the bound state. The ^{15}NH dipolar couplings show some reduction for the membrane-bound peptides. However, the coupling value along the NH bond is very sensitive to hydrogen bonding and, therefore, not entirely due to molecular motion (*50*).

DISCUSSION

The membrane affinity of the B18 peptide is manifested by its seven Leu residues that contribute a free energy of transfer from the aqueous environment (initial state) to the membrane interface (final state) of −3.92 kcal/mol (*51*). Altogether, a favorable free energy of transfer of −0.95 kcal/mol is obtained for all residues of B18, explaining the preference of the peptide for the membrane. The binding of B18 to zwitterionic membranes and its fusogenic activity is strongly enhanced by Zn^{2+} ions. These ions bind to the His-rich center of the peptide and increase the propensity of the peptide for the membrane by formation of a POPC/Zn^{2+}/B18 complex (*18*, *20*). Therefore, the structure and dynamics of B18 associated with zwitterionic membranes in the presence of Zn^{2+} were investigated in this study.

Membrane binding of soluble peptides or proteins very often leads to pronounced structure and mobility changes (*26*, *52*−*54*). When approaching a lipid membrane, the peptide experiences an environment of decreasing polarity, which significantly differs from the properties of the aqueous solvent. Fixed charges and the polar nature of the peptide backbone lead to an increase in Born repulsion upon membrane approach of the peptide (*55*). Consequently, membrane partitioning has only been observed for hydrogen-bonded secondary structures such as α-helices and oligomeric β-sheet elements, which significantly reduces the free energy of transfer from water to the membrane by 0.7 kcal/mol per amino acid (*51*, *56*).

In this study, secondary structure changes upon membrane binding of the B18 peptide have been determined quantitatively by solid-state NMR spectroscopy, which is the method of choice for the investigation of peptide binding to intact bilayer membranes. Since anisotropic interactions are not averaged out in solids, MAS in combination with specific isotopic labeling has to be applied to obtain structural data even for relatively small peptides.

Our solid-state NMR results for crystalline B18 showed a coil structure. The terminology "coil" is a bit misleading since it implies that the structure is "random" and thus poorly defined. This is, however, not the case for crystalline B18 since relatively narrow ^{13}Cα and ^{13}CO lines are observed, indicating that the peptide adopts a well-defined conformation with φ torsion angles for the three investigated Leu sites between −80° and −90°. Therefore, following the suggestion in ref *45*, we refer to coil structures for all molecular structures that are not α-helix or β-sheet.

When bound to a zwitterionic POPC membrane in the presence of Zn^{2+} ions, a structural change of B18 occurs. Both isotropic chemical shift measurements and the quantitative φ torsion angle determination indicate that membrane-bound B18 exhibits a parallel β-sheet-like structure. While folding and structural changes upon membrane binding are typically observed for fusion peptides (*4*, *52*), this result comes somewhat as a surprise because both solution NMR and CD spectroscopy have revealed an α-helical structure of B18 (*18*, *19*). However, in these measurements, the helical structure of B18 was found in membrane-mimicking solution (such as TFE) or when bound to detergent micelles. Since interface and curvature properties of micelles differ significantly from planar bilayers, it is understandable that the bilayer structure of the B18 peptide observed in this study is completely different. To resolve this contradiction, we have carried out isotropic chemical shift measurements that indicate the formation of β-sheet structures at high peptide concentration (Figure 6). Further, FTIR measurements are consulted, which have revealed that the B18 structure in lipid membranes in the presence of Zn^{2+} is α-helical at low (i.e., 1:50 B18:lipid) and β-sheet-like at high peptide concentration (i.e., 1:5 B18:lipid) (*20*).

In our measurements of the B18 structure and dynamics, a peptide to lipid ratio of 1:12 was used to simulate the fusion active state of the peptide in POPC membranes that appears to involve these high B18 concentrations (Figure 2). Therefore, we conclude that the parallel β-sheet arrangement found for membrane-associated B18 is the structure that the peptide assumes in the bilayer membrane at relatively high concentration.

^{2}H NMR order parameters of the lipid chains indicated that membrane binding of B18 in the presence of Zn^{2+} leads to significant perturbations of the lipid packing and membrane structure. The order parameter decrease upon B18 binding is particularly pronounced for the lower chain segments (Figure 4). Such order changes are typical signatures of penetration of the lipid water interface of the membrane by the bound peptide (*57*). Since only hydrogen-bonded structures can penetrate the lipid bilayer (*56*), it has to be concluded that the β-sheets of the B18 peptide oligomerize upon membrane binding in the presence of Zn^{2+} at high enough concentrations. Hydrogen bonding in β-sheet structures can be satisfied in parallel or antiparallel arrangements of individual sheets. Indeed, the φ torsion angles that we measured for the peptide all suggest that B18 forms a parallel β-sheet when bound to the membrane (Table 2). Although only three torsion angles have been measured in this study, the labels were distributed over the entire peptide. It is very unlikely that the three residues between L-4 and L-8 and the six residues between L-8 and L-15 would have a different secondary structure. The widths of the carbonyl and the Cα lines of the membrane-associated B18 peptide are very small (∼1−2 ppm), which indicates that there is little structural heterogeneity within the peptide (*6*).

It has been reported that peptide self-aggregation plays an important role in the course of action of fusogenic peptides (*8*, *11*, *28*). Oligomeric parallel β-sheets can penetrate the lipid membrane, which leads to a decrease in lipid chain order parameters (Figure 4). Such a shallow penetration of B18 causes a local destabilization of the membrane due to the introduction of curvature strain, which may finally lead to the formation of the fusion pore. Therefore, we hypothesize that structural changes and oligomerization into parallel β-sheets are necessary prerequisites for the fusogenic activity of membrane-bound B18.

In a previous study, the β-sheet structure of B18 has been considered "inactivated" to induce membrane fusion based on freeze−fracture electron microscopy results (*21*). This is in contradiction with our results that indicate that high B18 concentrations are required to induce fusion in POPC membranes. However, in ref *21*, the inactivated β-sheet state of B18 has been observed in the absence of Zn^{2+}, which is required to induce fusion. While this controversy cannot fully be resolved here, we note that there are several β-sheet-like fusion peptides that represent the active state in the course of the fusion event (*6*, *58*, *59*). Very recently, Weliky and co-workers have shown elegantly that artificial oligomerization of the fusion peptide gp41 from HIV-1 induced by a cross-linker leads to parallel β-sheet structures that show the full fusion activity even at very low peptide to lipid ratio (*58*).

An oligomeric β-sheet structural arrangement would also be consistent with the mobility changes of B18 observed upon Zn^{2+}-mediated membrane binding. The order parameters of the peptide backbone are relatively high. This is indicative of a rather rigid structure, while short peptides or secondary structure elements of proteins can acquire significant mobility (*57*, *60*, *61*). The relatively rigid peptide backbone is a consequence of the intermolecular hydrogen bonds that stabilize the parallel β-sheet arrangement of B18, similar to the β-barrel membrane protein OmpA (*62*). Only for B18 L-8 is a somewhat lower order parameter measured for the membrane-bound sample. This leucine residue is located at the Zn^{2+} binding site of the peptide. Zn^{2+} ions may slightly influence the intersheet hydrogen bonding, resulting in somewhat higher mobility.

The leucine side chains are not involved in hydrogen bonding. Consequently, their mobility is higher in the liquid-crystalline bilayer. The motion of the leucine side chains can be modeled as a superposition of wobbling in a cone and discrete jumps between different rotamers (*60*). According to X-ray investigations, for leucine side chains only two out of the nine possible rotamers are significantly populated (*63*). The continuous reduction of CH order parameters along the leucine side chain indicates that both χ_1 and χ_2 angles are flexible and the side chains are in fast exchange between the gauche$^+$-trans and the trans-gauche$^-$ conformation. The lower order parameters in the membrane-bound state may indicate different populations of the two rotamers but also larger amplitude wobbling motions of the side chains due to collisions with the highly mobile lipid molecules in the liquid-crystalline membrane.

All motions with correlation times much smaller than the inverse of the interaction strength scale down dipolar couplings. Therefore, the motions detected for the leucine residues in B18 must have correlation times much smaller than $\sim$40 μs. Typically, these segmental and side-chain motions are much faster with correlation times on the order of a few nanoseconds (*64*).

In summary, we have identified the structure of the membrane-bound B18 fusion peptide in the presence of Zn^{2+} at high peptide concentration to be an oligomeric parallel β-sheet. This structure is bound to the lipid−water interface of the membrane. Membrane binding is accompanied by a moderate increase in segmental mobility, which is particularly noteworthy for the side chains. Since oligomerization appears to be required during a fusion event, we hypothesize that the observed structural peptide arrangement and its impact on membrane structure and packing properties represent an active state in the course of action of the B18 fusion peptide. Indeed, according to a fusion assay, high peptide concentrations are required to induce fusion in zwitterionic POPC membranes in the presence of Zn^{2+}.

ACKNOWLEDGMENT

The authors thank Drs. A. Pampel and M. Findeisen for technical support with the HSQC experiment.

REFERENCES

1. Martin, I., and Ruysschaert, J. M. (2000) *Biosci. Rep. 20*, 483−500.
2. Israelachvili, J. N. (1992) *Intermolecular and surface forces*, Academic Press, London.
3. Sollner, T., Whiteheart, S. W., Brunner, M., Erdjument-Bromage, H., Geromanos, S., Tempst, P., and Rothman, J. E. (1993) *Nature 362*, 318−324.
4. Tamm, L. K., Han, X., Li, Y., and Lai, A. L. (2002) *Biopolymers 66*, 249−260.
5. Han, X., Bushweller, J. H., Cafiso, D. S., and Tamm, L. K. (2001) *Nat. Struct. Biol. 8*, 715−720.
6. Yang, J., Gabrys, C. M., and Weliky, D. P. (2001) *Biochemistry 40*, 8126−8137.
7. Curtain, C., Separovic, F., Nielsen, K., Craik, D., Zhong, Y., and Kirkpatrick, A. (1999) *Eur. Biophys. J. 28*, 427−436.
8. Kliger, Y., Aharoni, A., Rapaport, D., Jones, P., Blumenthal, R., and Shai, Y. (1997) *J. Biol. Chem. 272*, 13496−13505.
9. Pereira, F. B., Goni, F. M., Muga, A., and Nieva, J. L. (1997) *Biophys. J. 73*, 1977−1986.
10. Epand, R. M., Epand, R. F., Martin, I., and Ruysschaert, J. M. (2001) *Biochemistry 40*, 8800−8807.
11. Rapaport, D., and Shai, Y. (1994) *J. Biol. Chem. 269*, 15124−15131.
12. Hofmann, A., and Glabe, C. G. (1994) *Semin. Dev. Biol. 5*, 233−242.
13. Vacquir, V. D., Swanson, W. D., and Hellberg, M. E. (2002) *Dev., Growth Differ. 73*, 1−10.
14. Miraglia, S. J., and Glabe, C. G. (1993) *Biochim. Biophys. Acta 1145*, 191−198.
15. Kennedy, L., DeAngelis, P. L., and Glabe, C. G. (1989) *Biochemistry 28*, 9153−9158.
16. Glabe, C. G. (1985) *J. Cell Biol. 100*, 800−806.
17. Glabe, C. G. (1985) *J. Cell Biol. 100*, 794−799.
18. Ulrich, A. S., Otter, M., Glabe, C. G., and Hoekstra, D. (1998) *J. Biol. Chem. 273*, 16748−16755.
19. Glaser, R. W., Grune, M., Wandelt, C., and Ulrich, A. S. (1999) *Biochemistry 38*, 2560−2569.
20. Binder, H., Arnold, K., Ulrich, A. S., and Zschornig, O. (2000) *Biochim. Biophys. Acta 1468*, 345−358.
21. Ulrich, A. S., Tichelaar, W., Forster, G., Zschornig, O., Weinkauf, S., and Meyer, H. W. (1999) *Biophys. J. 77*, 829−841.
22. Stejskal, E. O., and Schaefer, J. (1976) *J. Am. Chem. Soc. 98*, 1031−1032.
23. Thompson, L. K. (2002) *Curr. Opin. Struct. Biol. 12*, 661−669.
24. Fu, R., and Cross, T. A. (1999) *Annu. Rev. Biophys. Biomol. Struct. 28*, 235−268.
25. de Groot, H. J. (2000) *Curr. Opin. Struct. Biol. 10*, 593−600.
26. Bechinger, B. (1999) *Biochim. Biophys. Acta 1462*, 157−183.
27. Smith, S. O., Aschheim, K., and Groesbeek, M. (1996) *Q. Rev. Biophys. 29*, 395−449.
28. Yang, J., Parkanzky, P. D., Khunte, B. A., Canlas, C. G., Yang, R., Gabrys, C. M., and Weliky, D. P. (2001) *J. Mol. Graphics Modell. 19*, 129−135.
29. Hope, M. J., Bally, M. B., Webb, G., and Cullis, P. R. (1985) *Biochim. Biophys. Acta 812*, 55−65.
30. Chen, P. S., Toribara, T. Y., and Warner, H. (1956) *Anal. Chem. 28*, 1756−1758.
31. Kay, L. E., Keifer, P., and Saarinen, T. (1992) *J. Am. Chem. Soc. 114*, 10663−10665.
32. Davis, J. H., Jeffrey, K. R., Bloom, M., Valic, M. I., and Higgs, T. P. (1976) *Chem. Phys. Lett. 42*, 390−394.
33. Huster, D., Arnold, K., and Gawrisch, K. (1998) *Biochemistry 37*, 17299−17308.

34. McCabe, M. A., and Wassall, S. R. (1995) *J. Magn. Reson. B 106*, 80−82.
35. Bennett, A. E., Rienstra, C. M., Auger, M., Lakshmi, K. V., and Griffin, R. G. (1995) *J. Chem. Phys. 103*, 6951−6958.
36. Munowitz, M. G., Griffin, R. G., Bodenhausen, G., and Huang, T. H. (1981) *J. Am. Chem. Soc. 103*, 2529−2533.
37. Schaefer, J., Stejskal, E. O., McKay, R. A., and Dixon, W. T. (1983) *J. Magn Reson. 52*, 123−129.
38. Hong, M., Gross, J. D., and Griffin, R. G. (1997) *J. Phys. Chem. 101*, 5869−5874.
39. Bielecki, A., Kolbert, A. C., and Levitt, M. H. (1989) *Chem. Phys. Lett. 155*, 341−345.
40. Struck, D. K., Hoekstra, D., and Pagano, R. E. (1981) *Biochemistry 20*, 4093−4099.
41. Köhler, G., Hering, U., Zschörnig, O., and Arnold, K. (1997) *Biochemistry 36*, 8189−8194.
42. Nagle, J. F. (1993) *Biophys. J. 64*, 1476−1481.
43. Wishart, D. S., and Sykes, B. D. (1994) *Methods Enzymol. 239*, 363−392.
44. Spera, S., and Bax, A. (1991) *J. Am. Chem. Soc. 113*, 5490−5492.
45. Wishart, D. S., Sykes, B. D., and Richards, F. M. (1991) *J. Mol. Biol. 222*, 311−333.
46. Xu, X. P., and Case, D. A. (2002) *Biopolymers 65*, 408−423.
47. Ye, C., Fu, R., Hu, J., Hou, L., and Ding, S. (1993) *Magn. Reson. Chem. 31*, 699−704.
48. Creighton, T. E. (1993) *Proteins. Structures and molecular properties*, W. H. Freeman, New York.
49. Webb, G. G., and Zilm, K. W. (1989) *J. Am. Chem. Soc. 111*, 2455−2463.
50. Zhao, X., Sudmeier, J. L., Bachovchin, W. W., and Levitt, M. H. (2001) *J. Am. Chem. Soc. 123*, 11097−11098.
51. White, S. H., and Wimley, W. C. (1999) *Annu. Rev. Biophys. Biomol. Struct. 28*, 319−365.
52. White, S. H., Ladokhin, A. S., Jayasinghe, S., and Hristova, K. (2001) *J. Biol. Chem. 276*, 32395−32398.
53. Engelman, D. M. (1996) *Science 274*, 1850−1851.
54. Cafiso, D. S. (1999) in *Current topics in membranes*, pp 197−228, Academic Press, San Diego.
55. Murray, D., Ben-Tal, N., Honig, B., and McLaughlin, S. (1997) *Structure 5*, 985−989.
56. Wimley, W. C., and White, S. H. (1996) *Nat. Struct. Biol. 3*, 842−848.
57. Koenig, B. W., Ferretti, J. A., and Gawrisch, K. (1999) *Biochemistry 38*, 6327−6334.
58. Yang, R., Yang, J., and Weliky, D. P. (2003) *Biochemistry 42*, 3527−3535.
59. Martin, I., Schaal, H., Scheid, A., and Ruysschaert, J. M. (1996) *J. Virol. 70*, 298−304.
60. Huster, D., Xiao, L., and Hong, M. (2001) *Biochemistry 40*, 7662−7674.
61. Prosser, R. S., and Davis, J. H. (1994) *Biophys. J. 66*, 1429−1440.
62. Arora, A., Abildgaard, F., Bushweller, J. H., and Tamm, L. K. (2001) *Nat. Struct. Biol. 8*, 334−338.
63. Batchelder, L. S., Sullivan, C. E., Jelinski, L. W., and Torchia, D. A. (1982) *Proc. Natl. Acad. Sci. U.S.A. 79*, 386−389.
64. Cross, T. A., and Opella, S. J. (1982) *J. Mol. Biol. 159*, 543−549.
65. Wishart, D. S., and Sykes, B. D. (1994) *J. Biomol. NMR 4*, 171−180.

BI034239E